Zachary Satterfield
Department of Mechanical Engineering,
Clemson University,
Clemson, SC 29634
e-mail: zsatter@g.clemson.edu

Neehar Kulkarni
Department of Mechanical Engineering,
Clemson University,
Clemson, SC 29634
e-mail: neehark@g.clemson.edu

Georges Fadel
Department of Mechanical Engineering,
Clemson University,
Clemson, SC 29634
e-mail: fgeorge@clemson.edu

Gang Li
Department of Mechanical Engineering,
Clemson University,
Clemson, SC 29634
e-mail: gli@clemson.edu

Nicole Coutris
Department of Mechanical Engineering,
Clemson University,
Clemson, SC 29634
e-mail: coutris@clemson.edu

Matthew P. Castanier
Analytics-Computational Methods & System
Behavior (CMSB) Team,
U.S. Army Tank Automotive Research,
Development, and Engineering Center (TARDEC),
Warren, MI 48397
e-mail: matthew.p.castanier.civ@mail.mil

Unit Cell Synthesis for Design of Materials With Targeted Nonlinear Deformation Response

A systematic unit cell synthesis approach is presented for designing metamaterials from a unit cell level, which are made out of linearly elastic constitutive materials to achieve tunable nonlinear deformation characteristics. This method is expected to serve as an alternative to classical Topology Optimization methods (solid isotropic material with penalization or homogenization) in specific cases by carrying out unit cell synthesis and subsequent size optimization (SO). The unit cells are developed by synthesizing elemental components with simple geometries that display geometric nonlinearity under deformation. The idea is to replace the physical nonlinear behavior of the target material by adding geometric nonlinearities associated with the deforming entities and thus, achieve large overall deformations with small linear strains in each deformed entity. A case study is presented, which uses the proposed method to design a metamaterial that mimics the nonlinear deformation behavior of a military tank track rubber pad under compression. Two unit cell concepts that successfully match the nonlinear target rubber compression curve are evaluated. Conclusions and scope for future work to develop the method are discussed. [DOI: 10.1115/1.4037894]

Keywords: metamaterials, design, unit cell, nonlinear

1 Introduction

Metamaterials are a class of artificial materials that are so named due to their designed purpose of achieving specific global properties different from those of their constitutive ones [1]. Useful behavior in metamaterials includes achieving unique mechanical properties such as a negative Poisson's ratio [2]), or addressing acoustic (e.g., sound transmission loss [3]), fluidic (e.g., permeable materials in fluid transport [4]), thermal (e.g., extreme thermal expansion [5]), or piezo-electric (e.g., hydrophone design [6]) requirements, among others. To engineer the mechanical properties of materials, metamaterials have been developed to minimize structural compliance in two-phase [7,8] and three-phase [9] materials, minimize Poisson's ratio [2], and target shear moduli [10], among others. Different from these applications, another class of metamaterial design problems stem from the need of mimicking the deformation behavior of nonlinear materials such as elastomers, or creating artificial materials to achieve a nonlinear deformation behavior that does not exist in natural materials. The development of such metamaterials would enable replacement with mechanical structures without the previously limiting failure modes while exhibiting the same functionality as the original structures. In addition, these metamaterials may greatly expand the design space in applications involving nonlinear deformation response and achieve new "predesigned" nonlinear responses of structural components. This class of metamaterials would be categorized under compliant structures that use material deformation to achieve desired mechanical characteristics [11]. In order to explore the different design techniques employed to design such metamaterials, a literature survey was carried out. Note that this work does not focus on truss-based structures, as one of the objectives is to achieve homogenous deformation behavior of the resulting metamaterials. In Ref. [12], the authors summarize the various methods used in the literature to design metamaterials for different applications. The numerical methodologies and optimization techniques used to design metamaterials are extensively reviewed in Ref. [13]. It is observed that computational methods such as topology optimization, size/shape optimization, and synthesis methods are among the most popular methods to design metamaterials.

Topology optimization has been successfully used, along with an inverse homogenization approach, to target prescribed material properties while minimizing cost (e.g., volume) across a variety of applications, see e.g., Refs. [10,14–16]. Sigmund defined and applied the inverse homogenization problem in Ref. [15] for using topology optimization to design metamaterials exhibiting arbitrary

Contributed by the Design Automation Committee of ASME for publication in the Journal of Mechanical Design. Manuscript received November 15, 2016; final manuscript received August 29, 2017; published online October 3, 2017. Assoc. Editor: Nam H. Kim.

constitutive properties in two-dimensional (2D) linear elastics. Sigmund then extended this work in Ref. [16] to three-dimensional linear elastics, showing examples of materials with targeted Poisson's ratio at extreme values of 1.0 and −1.0. The authors in Ref. [10] developed an alternative to the homogenization method, volume averaging, to design one- and two-layer metamaterials with targeted shear properties in linear elastics. Recently, the authors in Ref. [14] were able to design nonlinear mechanisms with prescribed stress–strain responses and materials that achieve prescribed Poisson's ratio across an axial strain range, $\varepsilon_i \in [0.00, 0.30]$.

Stress-based topology optimization is a vast field and work has been carried out in the past by various researchers to impose stress constraints while carrying out topology optimization. Cheng and Guo in Ref. [17] developed and applied a stress constraint for topology optimization by overcoming the singularity issue with an epsilon-relaxed formulation. Bruggi and Venini presented an alternate approach to enforcing stress constraints in Ref. [18] by using mixed finite element method that enables local stress constraints to be enforced more computationally efficiently. Le et al. in Ref. [19] developed a P-norm global stress constraint and a clustering technique to reduce the number of required adjoint sensitivity computations by reducing the number of total stress constraints. Holmberg et al. expanded on the clustering technique in Ref. [20] with "distributed stress" and "stress level" reclustering techniques that show improved local stress control while enforcing only a few constraints.

Two significant challenges that are yet to be explored in the design of metamaterial unit cells with topology optimization are consideration of the unit cell aspect ratio and the periodicity of the boundary conditions in all directions. In most traditional topological design problems, the design domain is determined during the problem's formulation and becomes fixed. However, the aspect ratio of an optimal unit cell, and therefore the design domain, for a given metamaterial design problem is unknown before solving. Therefore, this aspect ratio should be considered as a free variable throughout the design process. We have not found any research that considers this issue of unit cell aspect ratio when designing metamaterials with classical topology optimization (solid isotropic material with penalization or Homogenization). For the issue of boundary conditions, the general approach of topology optimization is valid and certainly preferred when the unit cell is small as compared to the overall domain. This unit cell to domain size ratio is one of the critical assumptions in homogenization theory [21]. When there are only three or four cells in each direction, the homogenization assumption is no longer valid since boundary conditions on the exterior of the domain are not similar to the ones on the unit cells inside the domain, thereby needing to be taken into account. Furthermore, as was shown in the paper by Czech et al. in Ref. [10] and by others in Refs. [22–26], sometimes the material design problems do not have to be periodic. In these cases, topology optimization cannot obtain a honeycomb or auxetic honeycomb structure if the domain is decomposed in a purely periodic manner. So, here again, the boundary conditions at the unit cell level have to be treated differently.

In this work, a unit cell synthesis approach is developed to design metamaterials to match targeted nonlinear uniaxial loading curves by synthesizing geometries at the unit cell level. This method is expected to serve as an alternative to classical topology optimization in specific cases by carrying out unit cell synthesis and subsequent size optimization (SO). As explained in Ref. [27], compliant mechanisms are bending-dominated with some sections in the structure undergoing significant bending or torsion. In Ref. [28], the authors have used nonlinear beam elements to model topologies of compliant mechanisms to achieve large deformations. On similar lines, the key idea of this method is to achieve a given nonlinear deformation behavior of the metamaterial through a combination of different geometric nonlinearities associated with different elemental geometries that undergo bending. The nonlinear deformation characteristics of the elemental components are obtained from the nonlinear finite element analysis of simple geometries. The elemental components in the unit cell are selected by comparing their nonlinear deformation characteristics with the target nonlinear deformation response. Finally, following a SO procedure, the optimized metamaterial is obtained.

The paper is organized as follows: The unit cell synthesis approach is described in Sec. 2. A case study demonstrating the design process and results is presented in Sec. 3. Finally, conclusions and scope for future work are discussed in Sec. 4.

2 The Unit Cell Synthesis Method

Figure 1 illustrates the unit cell synthesis method for metamaterial design. The scope of this method is limited to 2D geometries that are extruded in the third dimension. Thus, three-dimensional lattices are not considered. The method contains an iterative process of selecting and placing elemental components in a unit cell and then carrying out the tessellation of the unit cell into a metamaterial. A series and parallel connection analogy model is used to qualitatively predict the softening or stiffening deformation behavior of combined geometric entities and, in turn, to form the conceptual design of a representative volume element (RVE). Finally, a size optimization procedure involving a detailed

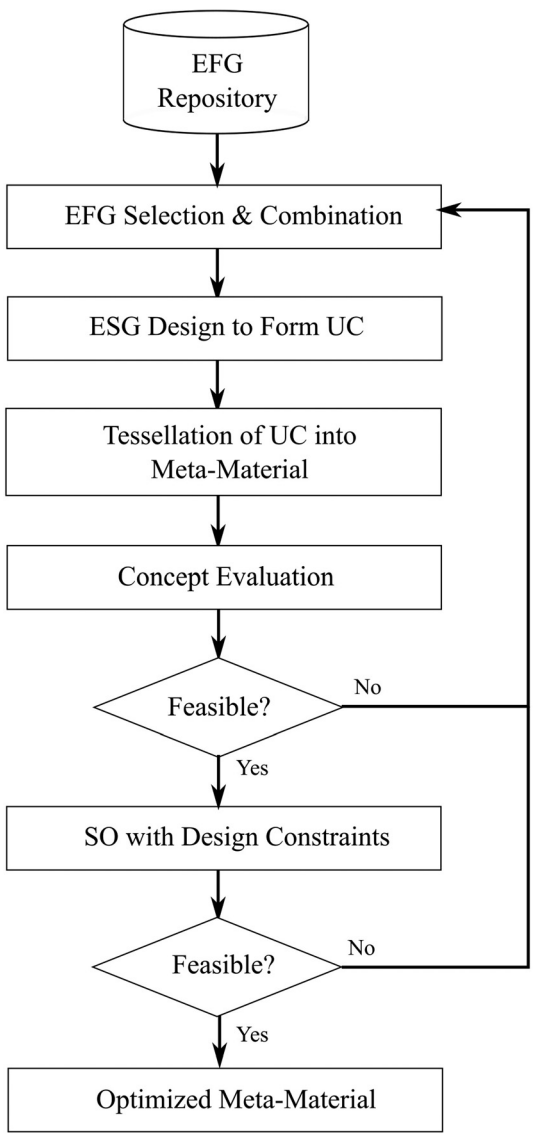

Fig. 1 Schematic of the unit cell synthesis method for metamaterial design

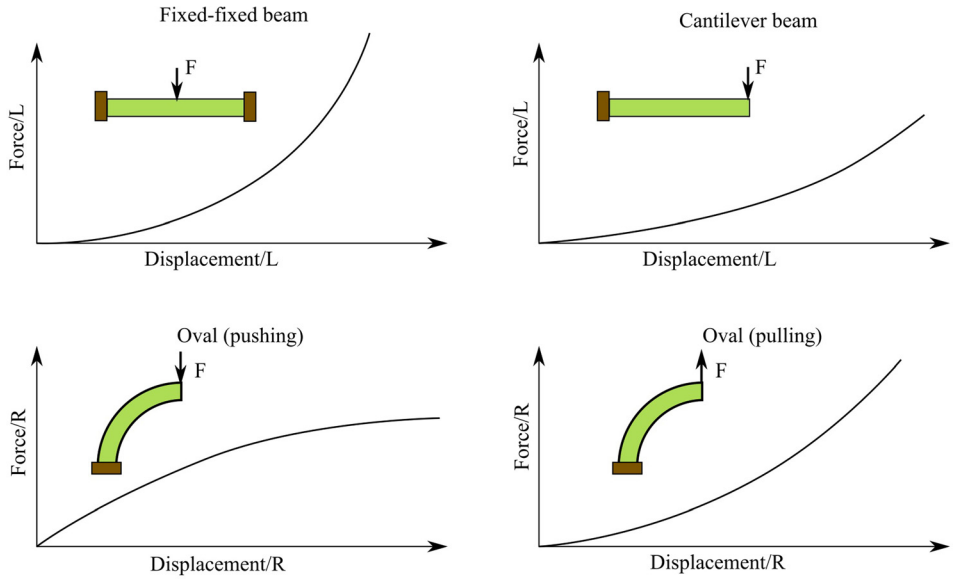

Fig. 2 EFGs and their general behavior (zeroth-order connection configuration)

nonlinear finite element analysis of the RVEs and metamaterial is performed to obtain the final design. The entire design process is divided into six steps. Each step is described in Secs. 2.1–2.6 in detail.

2.1 Step 1: Preparation of EFG Repository. An elemental functional geometry (EFG) is defined as a geometry whose deformation behavior is used to meet a desired response. In the unit cell synthesis method, the first step is to prepare a repository of simple elements whose deformation behavior is predetermined. Examples of EFGs include cantilever beams (CBs), fixed–fixed beams (FFBs), and oval structures (curved beams). The deformation behavior of the EFGs in case of large deformation is predetermined by using finite element analysis. Figure 2 shows the EFGs and their general deformation behavior when they are subjected to a concentrated load and undergo large deformation. The parameter sensitivities of their nonlinear deformation behavior are described in the Appendix. As shown in Fig. 2, while three of the deformation curves show stiffening characteristics with different magnitude of stiffening with respect to displacement, the oval EFG subjected to a pushing load has a reciprocal behavior—it softens as the applied load increases. These different and complimentary deformation behaviors of the EFGs allow the overall metamaterial behavior to be tuned toward the target curve by combining the deformation behavior of the EFGs.

2.2 Step 2: EFG Selection and Combination. The EFGs can be combined in different ways. In this work, the combinations are categorized by their configuration orders. If a single EFG is used in a unit cell, it is defined as a zeroth-order configuration as shown in Fig. 2. When two EFGs are combined together, it is referred to as a first-order connection configuration. The first-order connection configuration can be further categorized into parallel and series connection configurations, as shown in Fig. 3. When two first-order configurations, or a first-order and a zeroth-order configuration, are combined, it becomes a second-order connection configuration, as shown in Fig. 4. For linear springs with constant stiffness denoted by k, the effective stiffness for a first-order connection can be obtained as $k_{\text{eff}} = k_1 + k_2$ for parallel connections and $k_{\text{eff}} = (1/(1/k_1) + (1/k_2))$ for series connections. Using similar analogy, the EFGs with nonlinear stiffness can be combined in series or parallel to create different order connections. However, the net effective stiffness of such systems cannot be determined by simply using the above relations due to the nonlinearities and the complex boundary conditions involved. The series and parallel connection analogies shown in Figs. 3 and 4 are used to qualitatively determine the nonlinear force–displacement characteristics of the combined structures (e.g., softening and hardening behavior). The precise deformation of the connection configurations is determined by nonlinear finite element analysis. Although configurations of higher orders can be formed in a straightforward manner by following the definition, we only consider configurations up to the second order in this paper. It can be observed from the figures that the first few orders of connection configurations are already able to generate a wide spectrum of nonlinear deformation behavior of the resultant unit cell.

2.3 Step 3: ESG Design to Create Unit Cell. Along with the EFGs, the other required element to form a unit cell is the

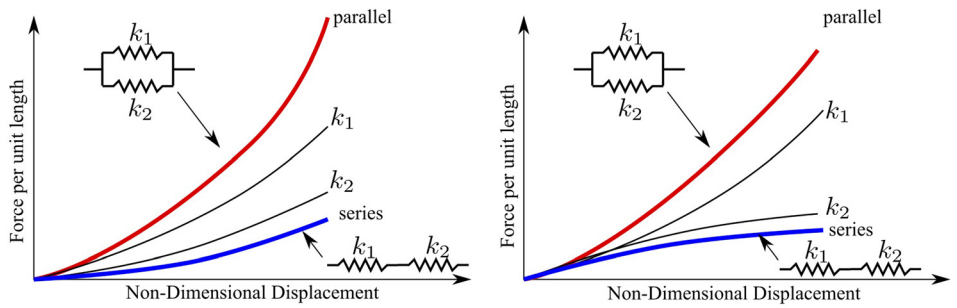

Fig. 3 First-order connection configuration

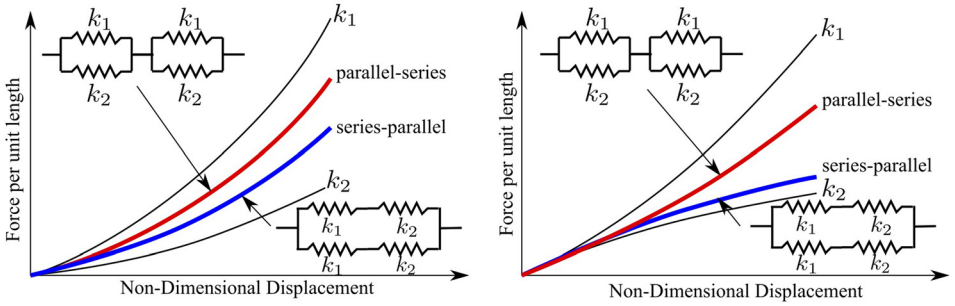

Fig. 4 Second-order connection configuration

elemental structural geometry (ESG). The ESGs are the structural components in a unit cell that serve as the support and/or rigid connection of the EFGs and adjacent unit cells. They typically have a much higher stiffness and do not interfere with the deformation of EFGs. Therefore, the next step is to design or select suitable ESGs that can lead to a unit cell design as long as they are designed within the purview of the following requirements:

(1) They must exhibit high stiffness and low deformation compared to the EFGs.
(2) They must complete the topology of the unit cell by connecting the EFG's between unit cells.

The first requirement of the ESG serves to isolate the tunable properties of the EFG while the second requirement serves to complete the unit cell in order to allow its tessellation into a metamaterial. The ESGs are intended to serve purely as structural entities that help shape the unit cell. Thus, it is not important to determine their deformation behavior beforehand.

2.4 Step 4: Tessellation into a Metamaterial. Once the base unit cell geometry has been designed, the metamaterial is formed by tessellating the unit cell multiple times in the x- and y-directions. For computational analysis and optimization purposes, an RVE of the metamaterial is constructed through tessellation. The number of unit cells in the RVE depends on several factors. It is well known that the fewer unit cells that exist in each direction, the more prominent the effect of boundary conditions. When the size of the metamaterial to be designed is much larger than the size of a unit cell (i.e., the target metamaterial can be considered as "bulk") and the boundary conditions can only be approximated, a tessellation with a relatively large number of unit cells is necessary for the performance analysis and optimization, and a convergence study is typically required to ensure that the deformation behavior of the RVE accurately represents the behavior of the bulk metamaterial. However, for applications with a restrictive design space, the dimension of the RVE can ultimately be determined by the size of the target structure, and this size becomes the driving factor in the allowable number of unit cells in the tessellation.

2.5 Step 5: Concept Evaluation. The mechanical properties of the metamaterial, as a continuum structure, may vary from that of the individual unit cell properties owing to the complex interactions between the unit cell boundaries and their connectivity. Since the homogenization techniques are not applied in this method and since the metamaterial is to be designed to have a target deformation behavior, which is different from that of its constitutive material, a means of determining the effective mechanical properties of the metamaterial must be determined. For a metamaterial RVE tessellated with a large number of unit cells, the metamaterial is evaluated based on the RVE's deformation characteristics. For a given target deformation behavior, typically described by one or multiple stress–strain curves, proper finite element analyses are performed on the RVE to obtain the

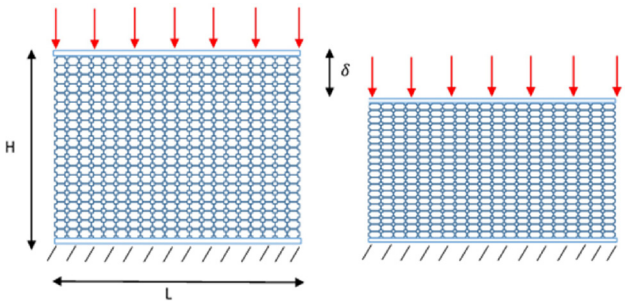

Fig. 5 Metamaterial with uniaxial loading (left) and after deformation (right)

force–displacement behavior of the metamaterial, as shown in Fig. 5. A metastrain can then be defined as the percentage of the "bulk" deformation (i.e., averaged displacement) of the metamaterial as

$$\text{meta} - \text{strain}\,(\varepsilon) = \%\ \text{"bulk"}\ \text{deformation} = \frac{\delta}{H}(100) \quad (1)$$

where δ is the displacement and H is the original height of the metamaterial. The metamaterial is subjected to a series of load cases corresponding to the range of the target curve(s). The metastrain is then calculated at each load case to determine the RVE deformation response, which can then be compared to the target curve for evaluation. For a metamaterial with restrictive design space, the definition of the metastrain remains the same. However, it should be noted that the averaged displacement obtained for such metamaterial RVE, which contains a relatively small number of unit cells, includes the effect of the material boundary. Thus, the boundary condition should be applied properly based on the actual boundary condition of the target structure.

While the complete deformation behavior of a nonlinear material can be defined by its nonlinear constitutive relation, it is often the case that one or two deformation modes dominate the deformation of the target material in a given application. Therefore, in most cases, it is sufficient to only take the stress–strain response of the target material in its dominant deformation mode(s) and find a metamaterial solution to match the dominant deformation behavior. With the identified target stress–strain response, the ability of unit cell parameters to be tuned to match the desired response is paramount before moving on to the next step. Determining this feasibility can be done by carrying out and analyzing a design of experiments study. This is a necessary intermediate step between the formation of the concept unit cell and optimizing unit cell parameters to meet the desired behavior.

If the concept unit cell with the selected EFG configuration is found to have a deformation behavior close to the desired material response during the concept evaluation stage, this concept unit cell is regarded as a "feasible" design. Otherwise, a different EFG configuration of the same or a higher order is selected and steps

2–5 are repeated with the new conceptual unit cell until feasibility is obtained. Note that higher order EFG configurations typically lead to an increase in the design parameters of the unit cell, which may impart more tuning ability to match the target behavior. While there may be multiple ways of combining the EFGs to achieve the desired deformation behavior, as shown in Figs. 3 and 4, it is logical that one starts with the lowest order configurations for the simplicity of the unit cell.

2.6 Step 6: Size Optimization With Design Constraints. An optimization of the dimensions of the EFGs and ESGs in the unit cell is conducted once the unit cell concept is deemed feasible. The SO procedure should be set up such that the parameterized concept unit cell design can be autonomously generated in computer-aided drawing, meshed, and run in a finite element code. This will allow the optimizer to iterate and converge the deformation response of the metamaterial toward that of the target response. The optimization setup can be mathematically written as

$$\min: f = \sum_{i=1}^{N} (\varepsilon_i^t - \varepsilon_i^c)^2 \tag{2}$$

where ε_i^t and ε_i^c are the target strain and the metastrain (i.e., the % deformation) of the metamaterial RVE, respectively, at the ith load level for a total of N load levels. Once the optimization is converged, the resulting metamaterial should have a deformation response close to that of the target. Note that the solution of such an optimization problem is typically not unique. The acceptance of the results obtained from the optimization run depends on their evaluation against the application-specific design constraints.

After a converged solution is obtained, the design constraints are analyzed to further rule out a potentially infeasible design of the metamaterial. Such design constraints include manufacturing feasibility, stress allowance, and the requirement of noncontact within permissible deformation limits. If a metamaterial design is deemed infeasible in this step, the starting design points for the optimization run may be changed and another SO carried out until the desired deformation behavior is obtained and the feasibility constraints are satisfied. However, if the SO iterations do not yield an acceptable optimal design, then the design process goes back to step 2. A different EFG configuration of the same or a higher order is selected and steps 2–6 are repeated with the new conceptual unit cell.

3 Case Study: Tank Track Pad Metamaterial

The U.S. Army employs the M1 Abrams tank as a tactical asset in combat and peace operations. The M1 Abrams tank uses the T158LL track pad to provide traction, sound dampening, and protect road surfaces [17]. The track pad consists of a homogenous rubber pad bonded to a steel backing plate. The current material that is used to manufacture the T158LL tank track pad is a carbon black-filled styrene-butadiene rubber (SBR). The use of carbon black reinforcements improves strength and abrasion resistance of SBR [18]. The most common mode of failure of the tank pad is through a process called blowout. During sustained high-speed operation, there is overheating and loss of strength of the rubber material due to hysteretic heat loss. The cyclic compressive loading of the track pad causes this hysteretic loss. The heat generated from hysteretic loss and other friction can exceed 300 °C during high-speed operation [19]. The costs associated with the repairs and replacements of tank track rubber are also very high [20]. While elastomers have the desired compliance required to provide traction and sound dampening since they exhibit high strains at low stress levels, they demonstrate hysteretic loss due to their viscoelastic nature. Therefore, a new material is sought to achieve high compliance while reducing or eliminating hysteretic heat loss.

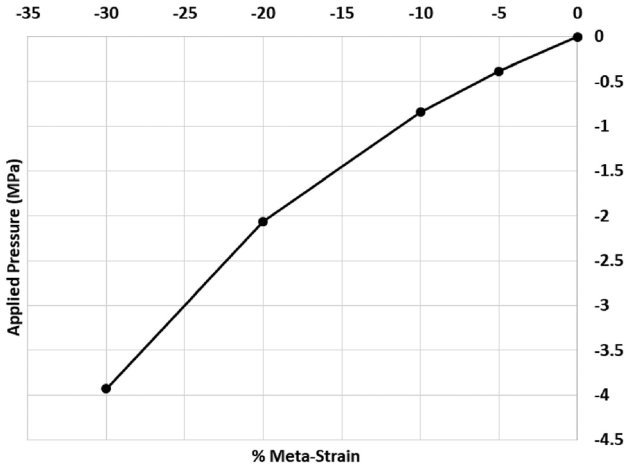

Fig. 6 Stress–strain curve of SBR under uniaxial compression

Since no alternative traditional material exists to fulfill the requirement of large compliance and low hysteretic loss, we propose to significantly reduce and possibly eliminate the hysteretic losses associated with the backer pad and ground pad by developing a metamaterial composed of linear elastic materials, which are inherently nonhysteretic. Since the predominant mode of deformation of the backer pad is compression, the design objective of the metamaterial is to achieve a defined nonlinear behavior under compression similar to the SBR in use. The material nonlinearity of the SBR is to be reproduced to achieve large, nonlinear, overall deformations by utilizing the geometric nonlinearity of the deforming EFGs in the unit cells while ensuring that each entity in the unit cell experiences small linear strains within the elastic limit of its constitutive material. Figure 6 shows the stress–strain relationship of the SBR in uniaxial compression obtained via experimental testing and subsequent curve fitting using a two-parameter Ogden model. It was determined in Ref. [29] that the backer pad experiences a maximum compressive strain of 20% as the tank wheels pass over it. Table 1 shows the target strain (metastrain) values for the metamaterial when subjected to compression, which are selected from the curve shown in Fig. 6. Each pressure value corresponding to the four strain levels acts as a separate load case for analyzing the metamaterial deformation response. Note that even though the metamaterial is to be designed to have a maximum compressive strain of 20%, the inclusion of the fourth load case corresponding to a strain of 30% ensures that the metamaterial behavior will closely resemble the overall behavior of the elastomer even beyond the targeted range.

3.1 "Brick" Design. In the first step of the unit cell synthesis method, a repository of the EFGs with their general deformation behavior is prepared as described in Sec. 2.1. In addition, a material selection study is performed to choose a material with a low ratio between elastic modulus to yield strength. In the context of the current application, a low value of this ratio indicates a higher ability to achieve large deformations before yielding. An aluminum, steel, or titanium alloy is chosen to be the possible metamaterial constitutive material. For the backer-pad design, the repository contains the three EFGs shown in Fig. 2 and the Appendix. A total

Table 1 Metamaterial target property values

Applied pressure (MPa)	% Metastrain
−0.3817	05.0
−0.8384	10.0
−2.0632	20.0
−3.9327	30.0

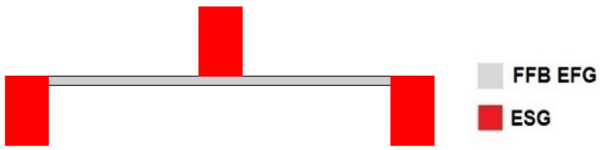

Fig. 7 FFB assembled with potential ESG to apply load and boundary conditions

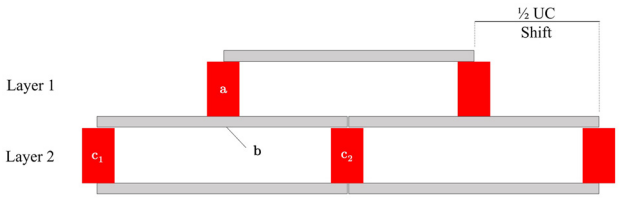

Fig. 8 Assembled EFG and ESG with periodicity for brick design

of four nonlinear deformation characteristics are available depending on the type and load of the EFGs. Note that the oval beam is treated as a single EFG despite exhibiting two different deformation behaviors based on the direction of the force acting on it. As shown in Fig. 6, the targeted compressive behavior indicates a stiffening of the material as the load increases, which is the primary behavior that is used to select an appropriate EFG. One such EFG that exhibits this behavior is the fixed–fixed beam as shown in Fig. 2. The parameter sensitivity analysis of this EFG, shown in Fig. 21 of the Appendix, shows that its geometric nonlinearity is highly tunable and has a general stiffening trend similar to the target response. The FFB is therefore selected as an EFG of the unit cell.

As described in Sec. 2.2, the design of the unit cell starts with a zeroth-order configuration of the selected EFG. Figure 7 shows a zeroth-order configuration of the EFG with an ESG imposing both the load and boundary conditions. The configuration can be made periodic through a shifted tiling process (i.e., tessellation), as shown in Fig. 8. From this process, an obvious unit cell is formed, denoted as the "brick" design. This conceptual design uses a metamaterial layer shift of half unit cell length to impose the load from the layer 1, via ESG "a," to cause bending in EFG "b." The load is distributed to both ESGs "c_1" and "c_2" in layer 2. ESGs "c_1" and "c_2" would then impose the load on the next layer. This load path continues throughout the metamaterial layer by layer where the ESGs act as the boundary support/connection and load source for the current and successive layer, respectively.

It is important to note that the ESG in the brick design follows both the ESG requirements. First, the ESG does not bend as compared to the EFG by acting as a strut to also prevent buckling. Second, the ESG provides connectivity between unit cells as it serves as the cell boundary in the current layer and load source for the successive layer. After a candidate unit cell is conceptualized, it is parameterized and a sensitivity analysis is performed to

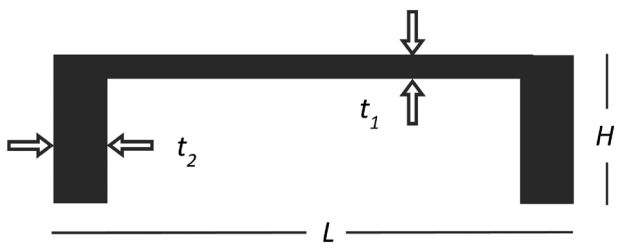

Fig. 9 Design variables in the brick unit cell

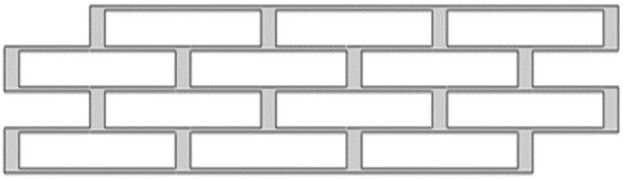

Fig. 10 Assembled brick design in 3 × 4 array

determine whether the candidate design can achieve the desired behavior. This concept evaluation step is performed by subjecting the tessellated metamaterial to a nonlinear finite element analysis. The four parameters of the unit cell are shown in Fig. 9. The initial values of the parameters are determined by using the sensitivity analysis results as shown in the Appendix, considering the manufacturability and required displacement limits. As shown in Fig. 9, the thickness t_1 and length $L - 2 \times t_2$ of the FFB are important for tuning the primary mode of deformation. The thickness t_2 and height $H - 2 \times t_1$ of the ESG are less important as long as there is negligible deformation in the ESG and the height is such that the deformation of the FFB does not make contact with that of the one beneath it. However, the overall height of the unit cell, H, changes the ratio in which the bulk deformation is calculated.

With the initial dimensions, the unit cells are tessellated into a metamaterial RVE for preliminary analysis, the number of unit cells and their dimensions are determined as per the constraints imposed by the application for which it is developed. For applications that do not have a size limit, a relatively large number of unit cells should be included in the RVE to ensure that it behaves like a "bulk" material and can be considered as homogeneous. For the track-pad design, based on the constraints of the pad size and manufacturing feasibility, the unit cells are tessellated into a 3×4 array as shown in Fig. 10. In this case, the compressive metastrain of the metamaterial pad is defined using Eq. (1), the metamaterial unit cells are designed such that this metastrain matches the uniaxial compression curve shown in Fig. 6. In other words, with the boundary effects taken into account, the compressive behavior of the metamaterial pad as a whole is required to reproduce that of the rubber pad.

In the next step, a two-level factorial study of variables L, H, and t_1 was carried out to determine the initial feasibility of the concept unit cell design. For a two-level factorial study experiment, if the combinations of k factors are investigated, the factorial design will consist of 2^k experiments [30]. It is sufficient to carry out a two-level factorial study as it was observed that the tessellated metamaterial's deformation response depends solely on the aspect ratios of the EFGs and the boundary conditions of the unit cells. The parametric study enables the determination of the relationship between the design parameters and the resultant response by using only a small set of combinations of design parameter values. While being discrete, the variation of the parameters covers the entire design space. In a two-level factorial study, each run is named for its combination of variable inputs of L, H, and t_1, respectively, where "1" represents a high value and "0" represents a low value and it accounts for all possible combinations of these values. The results are shown in Fig. 11. Note that, for the sake of brevity, only the results obtained with steel ($E = 210\,\text{GPa}$, $\rho = 7850\,\text{kg/m}^3$, $\nu = 0.30$) as the constitutive material are shown.

Although there are only eight simulation curves as shown in Fig. 11, they represent the metamaterial's response over the entire design space. It can be seen from the parametric study that the brick design exhibits a stiffening elastic behavior as the load increases. However, it is evident that no combination of parameters L, H, and t_1 will allow for convergence to the target behavior as the concept design exhibits a stronger stiffening behavior as compared to the target curve. Therefore, the brick design is not a feasible solution for the track pad.

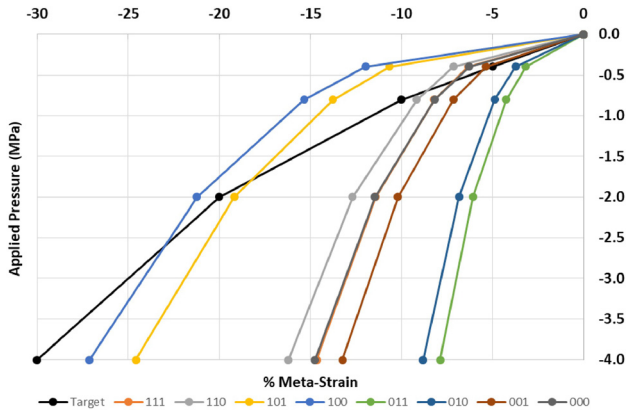

Fig. 11 Parametric study of the brick design (1: High Value, 0: Low Value)

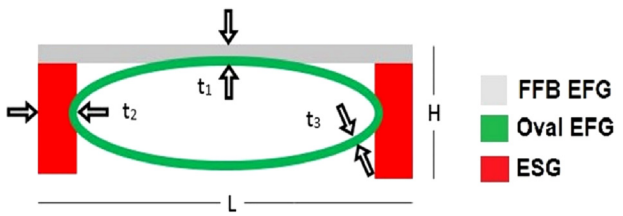

Fig. 12 BrickOval unit cell with elemental geometries and parameters

3.2 "Brick-Oval" Design. The results given in Fig. 11 indicate that the brick design with the zeroth-order configuration always has a stronger stiffening behavior compared to the target curve. A search in the repository shown in Figs. 2–4 indicates that the nonlinear behavior of the metamaterial can be tuned by multiple first- and second-order configurations. For a simple unit cell design, a first-order parallel configuration of an FFB and an oval EFG being pushed, as shown in Fig. 23 of the Appendix is selected to lower the stiffening strength of the metamaterial. Therefore, a BrickOval concept is developed by adding an oval EFG to the FFB EFG in a parallel fashion as shown in Fig. 12.

To ensure the same vertical displacement of the oval and FFB EFGs required by the parallel configuration, the oval geometry is implemented in the brick unit cell such that it is attached to the ESG and FFB EFG at the major and minor axes, respectively. The major and minor axes of the oval are therefore dependent on the shape of brick structure. Thus, the BrickOval unit cell only has a single additional parameter, t_3, the oval thickness. The 3×4 assembled BrickOval metamaterial is shown in Fig. 13 with an identical half-layer shift as the brick design.

A similar parameter sensitivity analysis is completed on the BrickOval design. The results are not included for brevity. It is observed that the oval thickness, t_3 allows the stiffening behavior of the metamaterial to be tuned. Then, SO is carried out to converge on the target curve. In order to perform SO, the unit cell geometry is parameterized according to the design variables and a script is developed to automatically generate the corresponding

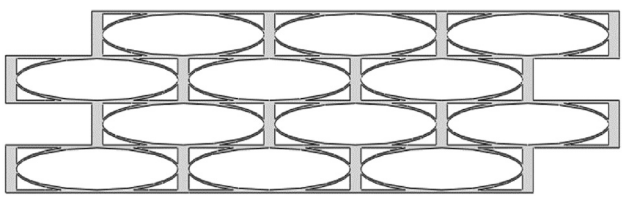

Fig. 13 Assembled BrickOval design in 3 × 4 array

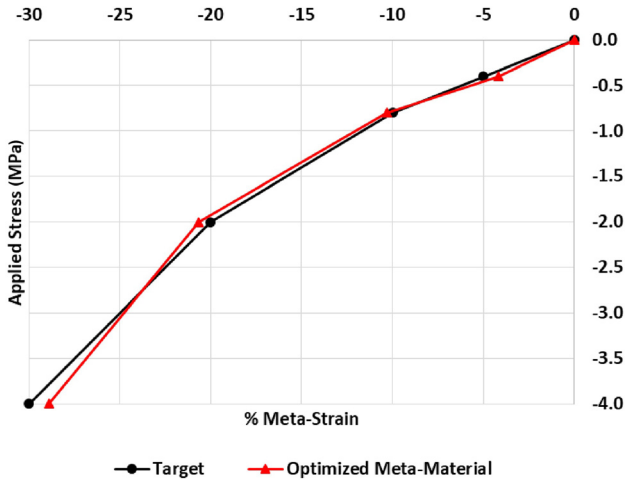

Fig. 14 Optimized BrickOval—target properties comparison

Table 2 Optimal design variable values of the BrickOval unit cell

Variables	Value (mm)
t_1	0.395
t_2	0.5
t_3	0.352
L	36.0
H	5.0

unit cell geometry in computer-aided drawing, tessellate it into a 2D array, mesh the geometry, submit the finite element simulation in Abaqus software, and extract the result. This script is further integrated into the optimization software modeFRONTIER where the optimization workflow is set to run each iteration with new unit cell parameters until convergence is achieved. A gradient-based optimization algorithm is implemented to carry out the size optimization. After 340 function evaluations, the resulting metamaterial behavior of the BrickOval design is shown to be converged to that of the target in Fig. 14. The optimal design variable values of the BrickOval design are given in Table 2.

The converged compression curve indicates initial feasibility of the BrickOval design. The obtained design is then evaluated against the design constraints, which include manufacturability and maximum stress requirements. Unfortunately, the maximum finite elemental von-Mises stress in the deformed structure at the maximum operating metastrains (i.e., 20%) is observed to exceed the yield stress for all of the three candidate constitutive elastic

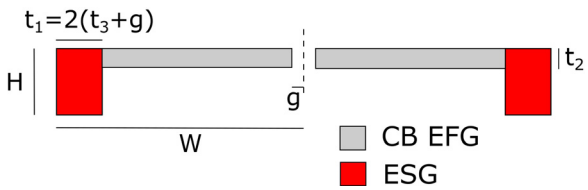

Fig. 15 Cantilever unit cell with elemental geometries and design variables

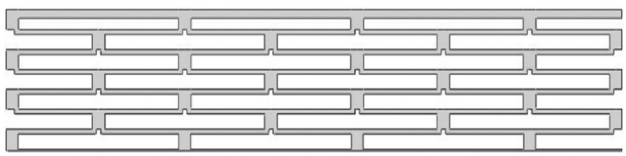

Fig. 16 Assembled cantilever design in 3 × 6 array

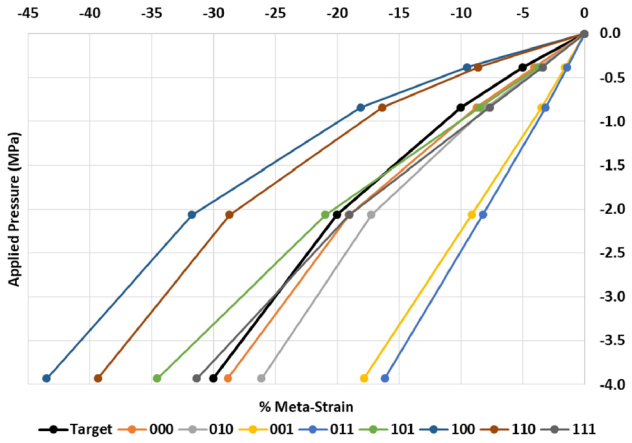

Fig. 17 Parametric study of cantilever design (1: High Value, 0: Low Value)

materials (aluminum, steel, and titanium alloys). The optimal design also violates the manufacturing constraints set for the thickness of the EFGs ($\geq$1 mm) [31]. Therefore, physical implementation of the BrickOval design as a replacement to the existing rubber track pad is proven to be infeasible.

3.3 "Cantilever" Design. After the unsuccessful attempt with the BrickOval design, the metamaterial design process goes back to the second step: selection of a configuration with new EFGs. It is shown in Fig. 22 of the Appendix that, compared to the FFB, the cantilever beam EFG also exhibits a stiffening elastic behavior, while allowing a larger deflection with a smaller strain in the beam. Therefore, in the third iteration of the metamaterial pad design, CB is chosen and the first-order parallel configuration is used as the initial design to make the unit cell symmetric. Figure 15 shows a unit cell constructed with two half-length beams acting as the EFG with five independent design variables. It is similar to the brick unit cell. However, the gap between the beam

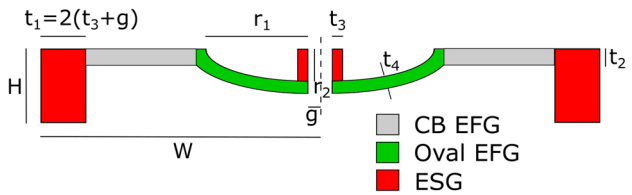

Fig. 18 CantiOval unit cell with elemental geometries and design variables

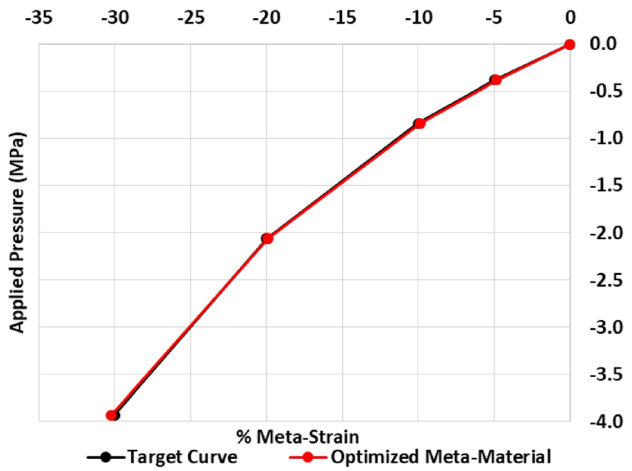

Fig. 19 Optimized CantiOval—target properties comparison

tips introduced by the variable "g" gives a relaxed boundary condition to the half-beams, allowing them to deflect like cantilever beams.

The ESGs are constructed as per the requirements mentioned in Sec. 2.3. The ESG is constructed such that $2 * (t_3 + g) = t_1$, making t_1 a dependent variable. Thus, the overall unit cell dimensions are $2W \times H$. The unit cell is then tessellated into a 3×6 array with a half unit cell shift similar to the earlier designs as shown in Fig. 16. Note that the current geometry of the unit cell requires additional face sheets on top and bottom of the assembly to allow uniform load and boundary conditions to be applied, respectively.

Since the variable t_1 is made considerably thicker as per ESG requirements and variables g and t_3 are dependent on it, the variables W, H, and t_2 are considered for parameter sensitivity analysis. The variables W and t_2 account for the aspect ratio of the cantilever beam. Variable H determines the height of the unit cell, which is directly related to metastrain of the metamaterial (Eq. (1)). It also ensures that there is no contact of the cantilever beam with the one in the unit cell beneath it during deformation. The parameter sensitivity analysis is carried out with 2D finite element analysis of the metamaterial using two-level factorial study as discussed in Sec. 3.1. Figure 17 shows the results of the parameter sensitivity study.

Based on the results shown in Fig. 17, it is found that the target nonlinear behavior could be achieved by using the configuration shown in Fig. 16. It is deemed to be a feasible concept design and the SO step is carried out next. However, the SO result indicates that the target curve can only be matched at high values of aspect ratio of the half-length beams. This behavior is in accordance with the results of the sensitivity study presented in Sec. A.2. On further analysis, it is observed that development of the unit cell (step 6) to match the target curve leads to violation of overall dimensional, manufacturing or stress constraints depending on how the design parameters are modified during the optimization process. For example, if the aspect ratio of the CBs is to be increased, keeping the length of the beams constant so as to constrain the overall width of the pad, the thickness of the beam has to be reduced to a point where it violates the manufacturing constraint ($\leq$ 1 mm) [31]. Hence, this unit cell design fails the evaluation against the design constraints of the track-pad application. The results are not shown here for the sake of brevity.

3.4 "Canti-Oval" Design. From the sensitivity study and the optimization results obtained from the earlier design, it is observed that the CB configuration has a lower rate of stiffening compared to the target curve. Thus, similar to the BrickOval design, based on the deformation characteristics of the configurations in the repository, the stiffening rate is to be tuned up by incorporating an EFG with a higher stiffening rate into the current configuration. A suitable choice is the second-order series-parallel configuration as shown in Fig. 4. The oval shape with a pulling deformation (stiffening) is selected as the second EFG. Figure 18 shows the EFG and ESG regions within the newly conceptualized unit cell. On each side, there is a series configuration of the CB

Table 3 Optimal design variable values of the CantiOval unit cell

Variables	Value (mm)
W	21.7
H	3.572
g	0.2
t_1	4.0
t_2	1.4
t_3	1.8
t_4	1.1
r_1	15.8
r_2	0.68

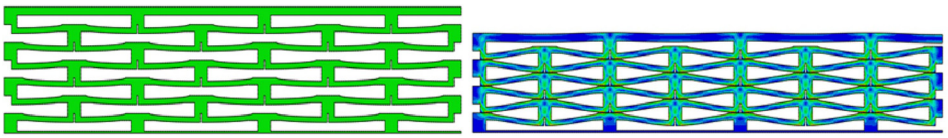

Fig. 20 Optimized CantiOval metamaterial

EFG and Oval EFG. The two sides act as springs in parallel when subjected to the load exerted from the ESG that acts on the center after the tessellation is carried out. The overall unit cell dimensions remain unchanged at $2W \times H$.

The incorporation of the oval shape leads to three additional design variables—r_1, r_2, and t_4—which are expected to impart more control in achieving the targeted nonlinear deformation behavior. Variable r_1, which is the major radius of the oval, also determines the length ratio i.e., the distribution of the CB EFG and Oval EFG within the unit cell. The unit cell is then tessellated into a 3×6 array to form the metamaterial structure. In the concept evaluation step, the parameter sensitivity analysis indicates that the nonlinearity could be tuned to match the target behavior. The results are not included for the sake of brevity. The parameters are then optimized using SO and the resulting compression plot is shown in Fig. 19 with optimized design variable values as shown in Table 3.

Figure 20 (left) shows the optimized metamaterial structure obtained. The series-parallel configuration of the CB and oval EFGs enabled successful matching of the nonlinear rubber compression curve. The subsequent evaluation of the obtained metamaterial against the design constraints of the track pad shows that the stresses developed within the optimized structure are within the permissible limits for the titanium alloy (maximum von Mises stress = 879 MPa, which is 80% of the Yield Strength), but not for aluminum and steel. The von Mises stress distribution in the deformed titanium alloy metamaterial structure at 20% compressive metastrain is shown in Fig. 20 (right). In addition, the minimum thickness of the elements in the unit cell is well above the manufacturing tolerances for the application. Thus, the CantiOval design using the titanium alloy as the constitutive linear elastic material is chosen as the most suitable tank track pad replacement.

4 Conclusions

This work introduces a novel technique referred to as the "unit cell synthesis method" for developing unit cell-based metamaterial structures with tunable nonlinear deformation characteristics. The proposed method enables a systematic development of unit cell structures using simple elemental geometries where a global deformation nonlinearity can be "designed" via a combination of geometric nonlinear deformation of the elemental geometries. Subsequent size optimization is performed on the unit cell design, ensuring that the metamaterial response converges to the targeted nonlinear response. The optimized metamaterial is further evaluated against application-specific design constraints before it can be accepted as a valid design.

A case study is discussed where the method is implemented to design a metamaterial to mimic the nonlinear deformation behavior of a rubber tank track pad. The purpose of this case study is to validate the method for designing a linear elastic material-based metamaterial to achieve a given nonlinear deformation behavior. The target of the optimization is to match the deformation behavior of the rubber pad under compression. The yielding failure is considered as a feasibility constraint in the optimization process. The resultant design computed from the optimization process was checked against the allowable stress of the constituent linear elastic material. In the current work, three metal materials are considered with aluminum, steel, and titanium alloys. Through optimization, both the BrickOval and Cantilever designs can match the target deformation curve. However, they are both deemed infeasible designs due to the excessive local elemental stresses under a 20% metastrain. Finally, the CantiOval design is shown to be a feasible design when titanium alloy is used as the constituent material. In this work, the failure due to fatigue is not considered. However, it will be investigated in future work.

While the effectiveness of the Unit Cell Synthesis approach is demonstrated, several improvements can be made to the proposed method. This work considers only three types of EFGs with four deformation characteristics. Additional EFGs such as "L"-shaped, cross-shaped, and variable thickness EFGs, among others, can be included in the repository to expand the potential design space this method explores. Additional EFG connection configurations can also be explored for targeting higher order and more complex nonlinearities. The proposed method can be further improved by including design guidelines to develop unit cells with special features such as filets so as to avoid stress concentrations. While the size optimization procedure is fully automated once a concept unit cell design has been developed, it is necessary to develop algorithms to enable automation of the concept unit cell synthesis to accelerate the design process. Furthermore, a multi-objective optimization process that optimizes the stresses, manufacturability, and dimensions of the EFGs simultaneously should be developed to further decrease required iterations to achieve an application-ready design solution. Finally, the method is presented in this work to target a single deformation curve. It is expected to be extended to simultaneously target curves of multiple deformation modes such as tension, compression, and shear.

Acknowledgment

The authors would like to thank the reviewers for their extensive feedback that enabled deeper justification and clarity of the ideas presented herein.

UNCLASSIFIED: Distribution Statement A. Approved for public release; distribution is unlimited.

Funding Data

- United States Army Tank Automotive Research, Development and Engineering Center (TARDEC).
- Automotive Research Center (ARC), University of Michigan.

Appendix: Example EFGS and Their Sensitivities

The purpose of this sensitivity analysis is for the designer to understand the effect of each parameter of the EFG on its geometric nonlinearity. Therefore, the designer can select and use EFGs according to their ability to match the required behavior. The sensitivity analysis is carried out by performing nonlinear finite element analysis on simple entities as shown below. Since the force–displacement characteristics of these different entities are only used qualitatively to design the unit cells, it is sufficient to consider their general deformation behavior and trend for a single constitutive material. In this case, all the entities are modeled with steel as their constitutive material.

A.1 Fixed–Fixed Beam. A fixed–fixed beam with length L and height h and unit depth is shown in Fig. 21. A beam with $L/h = 20$ is used as a datum for the sensitivity study. Only the effects of increasing L keeping h constant are presented in the study. It can be seen from the plot that the fixed–fixed beam shows stiffening behavior at higher force magnitudes as the aspect ratio L/h increases.

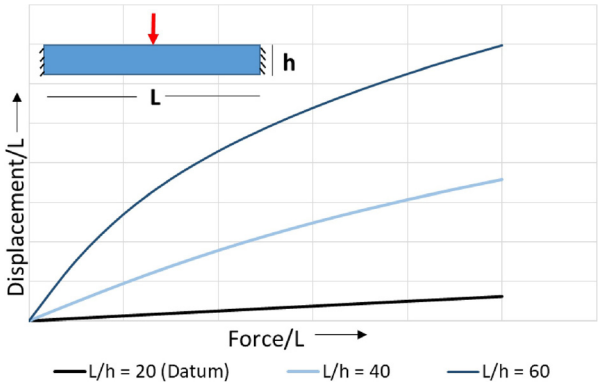

Fig. 21 Force–displacement response of FFB with parameter sensitivities

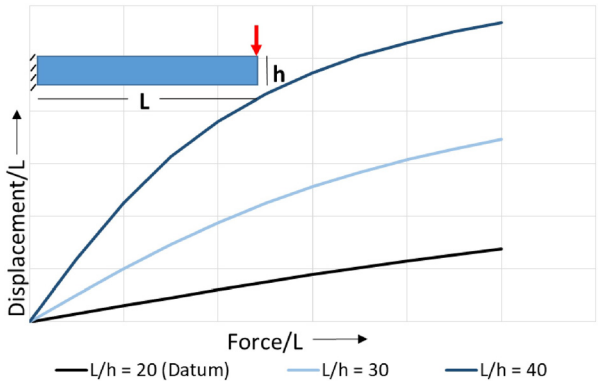

Fig. 22 Force–displacement response of Cantilever beam with parameter sensitivities

A.2 Cantilever Beam. Figure 22 shows the sensitivity results of a cantilever beam with varying aspect ratio L/h. Beam with aspect ratio $L/h = 20$ is considered as a datum. It is common knowledge that increasing the aspect ratio L/h keeping h constant will develop lower stresses as compared to reducing h and keeping L constant. Hence, only one scenario is evaluated in the analysis. It can be seen that the beam exhibits nonlinear stiffening force–displacement relationship at higher values of aspect ratio with increase in force magnitude.

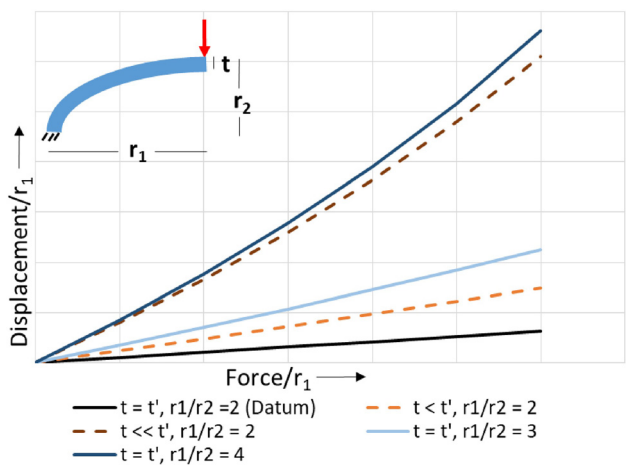

Fig. 23 Force–displacement response of Oval-1 beam with parameter sensitivities

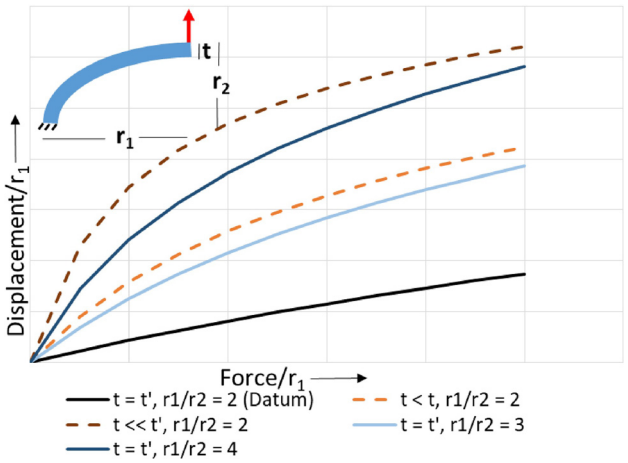

Fig. 24 Force–displacement response of Oval-2 beam with parameter sensitivities

A.3 Oval Beam. An oval beam with major and minor radii r_1 and r_2, respectively, with thickness t and unit depth is considered for design sensitivity study. Oval beam with ratio $r_1/r_2 = 2$ with $t = t'$ is considered as a datum. The sensitivity study is performed in two ways. First, keeping r_1 and r_2 constant, the effects of changing the thickness t are determined. Second, keeping the thickness constant, the ratio is changed. For the second case, only the effects of increasing r_1 and keeping r_2 constant are presented. The oval geometry is classified into two types depending on the direction of the force applied:

A.3.1 Oval-1. The oval beam with force acting downward as shown in Fig. 23 experiences softening behavior with increase in force magnitude. Both, reducing the beam thickness and increasing the ratio, increase the nonlinear softening behavior of the oval beam.

A.3.2 Oval-2. As opposed to the Oval-1 case, the oval beam with force acting upward as shown in Fig. 24 shows stiffening behavior with increase in force magnitude. Similar to Oval-1, the non-linear behavior is enhanced as the thickness t decreases or ratio increases.

References

[1] Walser, R. M., 2001, "Electromagnetic Metamaterials," *Proc. SPIE*, **4467**, pp. 1–15.

[2] Larsen, U. D., Sigmund, O., and Bouwstra, S., 1997, "Design and Fabrication of Compliant Micromechanisms and Structures With Negative Poisson's Ratio," J. Microelectromech. Syst., **6**(2), pp. 99–106.

[3] Galgalikar, R., 2012, "Design Automation and Optimization of Honeycomb Structures for Maximum Sound Transmission Loss," Master's thesis, Clemson University, Clemson, SC.

[4] Guest, J. K., and Prévost, J. H., 2007, "Design of Maximum Permeability Material Structures," Comput. Methods Appl. Mech. Eng., **196**(4–6), pp. 1006–1017.

[5] Sigmund, O., and Torquato, S., 1997, "Design of Materials With Extreme Thermal Expansion Using a Three-Phase Topology Optimization Method," J. Mech. Phys. Solids, **45**(6), pp. 1037–1067.

[6] Sigmund, O., Torquato, S., and Aksay, I. A., 1998, "On the Design of 1-3 Piezocomposites Using Topology Optimization," J. Mater. Res., **13**(4), pp. 1038–1048.

[7] Bendsøe, M. P., and Kikuchi, N., 1988, "Generating Optimal Topologies in Structural Design Using a Homogenization Method," Comput. Methods Appl. Mech. Eng., **71**(2), pp. 197–224.

[8] Bendsøe, M. P., and Sigmund, O., 2004, *Topology Optimization: Theory, Methods, and Applications*, Springer, Berlin.

[9] Gibiansky, L. V., and Sigmund, O., 2000, "Multiphase Composites With Extremal Bulk Modulus," J. Mech. Phys. Solids, **48**(3), pp. 461–498.

[10] Czech, C., Guarneri, P., and Fadel, G., 2012, "Meta-Material Design of the Shear Layer of a Non-Pneumatic Wheel Using Topology Optimization," ASME Paper No. DETC2012-71340.

[11] Berglind, L. A., and Summers, J. D., 2014, "Direct Displacement Synthesis Method for Shape Morphing Skins Using Compliant Mechanisms," ASME Paper No. DETC2010-28546.

[12] Fazelpour, M., and Summers, J. D., 2013, "A Comparison of Design Approaches to Meso-Structure Development," ASME Paper No. DETC2013-12295.
[13] Yoder, M., Satterfield, Z., Fazelpour, M., Summers, J. D., and Fadel, G., 2015, "Numerical Methods for the Design of Meso-Structures: A Comparative Review," ASME Paper No. DETC2015-46289.
[14] Wang, F., Sigmund, O., and Jensen, J. S., 2014, "Design of Materials With Prescribed Nonlinear Properties," J. Mech. Phys. Solids, **69**(1), pp. 156–174.
[15] Sigmund, O., 1994, "Materials With Prescribed Constitutive Parameters: An Inverse Homogenization Problem," Int. J. Solids Struct., **31**(17), pp. 2313–2329.
[16] Sigmund, O., 1995, "Tailoring Materials With Prescribed Elastic Properties," Mech. Mater., **20**(4), pp. 351–368.
[17] Cheng, G. D., and Guo, X., 1997, "ε-Relaxed Approach in Structural Topology Optimization," Struct. Optim., **13**(4), pp. 258–266.
[18] Bruggi, M., and Venini, P., 2008, "A Mixed FEM Approach to Stress-Constrained Topology Optimization," Int. J. Numer. Methods Eng., **73**(12), pp. 1693–1714.
[19] Le, C., Norato, J., Bruns, T., Ha, C., and Tortorelli, D., 2010, "Stress-Based Topology Optimization for Continua," Struct. Multidiscip. Optim., **41**(4), pp. 605–620.
[20] Holmberg, E., Torstenfelt, B., and Klarbring, A., 2013, "Stress Constrained Topology Optimization," Struct. Multidiscip. Optim., **48**(1), pp. 33–47.
[21] Hassani, B., and Hinton, E., 1998, "A Review of Homogenization and Topology Optimization I—Homogenization Theory for Media With Periodic Structure," Comput. Struct., **69**(6), pp. 707–717.
[22] Czech, C., 2012, "Design of Meta-Materials Outside the Homogenization Limit Using Multiscale Analysis and Topology Optimization," Ph.D. dissertation, Clemson University, Clemson, SC.
[23] Czech, C., Guarneri, P., Thyagaraja, N., and Fadel, G., 2015, "Systematic Design Optimization of the Metamaterial Shear Beam of a Nonpneumatic Wheel for Low Rolling Resistance," ASME J. Mech. Des., **137**(4), p. 041404.
[24] Gonella, S., and Ruzzene, M., 2008, "Homogenization and Equivalent In-Plane Properties of Two-Dimensional Periodic Lattices," Int. J. Solids Struct., **45**(10), pp. 2897–2915.
[25] Diaz, A. R., and Bénard, A., 2003, "Designing Materials With Prescribed Elastic Properties Using Polygonal Cells," Int. J. Numer. Methods Eng., **57**(3), pp. 301–314.
[26] Lipperman, F., Fuchs, M. B., and Ryvkin, M., 2008, "Stress Localization and Strength Optimization of Frame Material With Periodic Microstructure," Comput. Methods Appl. Mech. Eng., **197**(45–48), pp. 4016–4026.
[27] Wang, H. V., 2005, "A Unit Cell Approach for Lightweight Structure and Compliant Mechanism," Ph.D. thesis, Georgia Institute of Technology, Atlanta, GA.
[28] Joo, J., and Kota, S., 2004, "Topological Synthesis of Compliant Mechanisms Using Nonlinear Beam Elements," Mech. Based Des. Struct. Mach., **32**(1), pp. 17–38.
[29] Dangeti, V. S., 2014, "Identifying Target Properties for the Design of Meta-Material Tank Track Pads," Igarss, Master's thesis, Clemson University, Clemson, SC.
[30] Lundstedt, T., Seifert, E., Abramo, L., Thelin, B., Nyström, Å., Pettersen, J., and Bergman, R., 1998, "Experimental Design and Optimization," Chemom. Intell. Lab. Syst., **42**(1–2), pp. 3–40.
[31] Merriam, E. G., Jones, J. E., and Howell, L. L., 2014, "Design of 3D-Printed Titanium Compliant Mechanisms," 42nd Aerospace Mechanisms Symposium, Greenbelt, MD, May 14–16, pp. 169–174.